

## Range, distribution, and stopping power of 800-keV $^{14}\text{N}^+$ ions implanted in metals from $Z_2 = 22$ to $Z_2 = 32$

Donald G. Simons, David J. Land, James G. Brennan,\* and Matt D. Brown

Naval Surface Weapons Center, White Oak, Silver Spring, Maryland 20910

(Received 2 June 1975; revised manuscript received 25 August 1975)

Concentration distributions of 800-keV  $^{14}\text{N}^+$  ions implanted in metallic targets from titanium ( $Z_2 = 22$ ) through germanium ( $Z_2 = 32$ ) were determined from  $\gamma$ -ray-yield distributions using the  $^{14}\text{N}(p,\gamma)^{15}\text{O}$  resonance reaction at 1061.0 keV. Comparison of the first and second moments of these distributions with those predicted by the theory of Lindhard, Scharff, and Schiott (LSS) shows that the measured distributions are generally shallower and narrower. In addition, the measured distributions are strongly skewed such that their concentrations fall off more rapidly for deeper target layers. Values for the third moment of these distributions are also presented. We have attributed the discrepancies between the measured and predicted distributions to the behavior of the electronic stopping power,  $S_e$ . Values of  $S_e$  for the targets studied here were determined by altering the LSS value of  $S_e$  for each target by a multiplicative constant such that the predicted projected range is equal to the first moment of the measured distribution. With this adjustment, the predicted range straggling agrees closely with the measured second moments. The adjusted values of  $S_e$  exhibit a  $Z_2$  dependence which is not accounted for in either the LSS or Firsov pictures of electronic stopping power. Increases in the LSS values by as much as 60% are needed to describe the measured distributions. The  $Z_2$  dependence of  $S_e$  observed here suggests that there is an oscillatory behavior similar to the  $Z_1$  dependence previously reported by Ormrod, MacDonald, and Duckworth, and by Hvelplund and Fastrup.

### I. INTRODUCTION

Studies of the passage of heavy charged particles through matter are of considerable practical as well as theoretical interest. It is desirable to advance our understanding of the range and range straggling and, more generally, of the shape of the concentration profiles of implanted heavy ions. One can estimate such distributions on the basis of theoretical calculations such as the well-known theory of Lindhard, Scharff, and Schiott<sup>1</sup> (LSS). However, it is desirable to determine the accuracy of such calculations in a wide variety of situations. In addition, investigations of this kind provide theoretical insight into the fundamental atomic collision processes that take place between the incident ions and the target atoms. Indeed, the distribution of the ions depends on the details of the atomic cross sections and may be helpful in establishing their form.

The theory developed by Lindhard and his collaborators consists of two parts, a transport theory<sup>1</sup> and an atomic collision theory.<sup>2,3</sup> From the transport theory, values of the projected range of the distribution (the centroid or first moment of the distribution) and the straggling (the variance or second moment of the distribution) can be calculated. A Gaussian concentration distribution having this centroid and variance is generally assumed. The equations for the higher moments, which give rise to, e.g., a skewness in the distribution, are available but have not been solved.

Two kinds of atomic collision processes are considered to be important in the LSS theory: the

elastic scattering of the incident ions from the target atoms considered as screened nuclei (namely, nuclear stopping), in which energy is lost to the recoil atom, and the inelastic scattering of the ion from the target electrons (namely, electronic stopping), in which energy is lost to the excitation and ionization of both projectile and target atoms. Lindhard *et al.*<sup>2,3</sup> have given specific analytic forms for the stopping powers for both processes. Additionally, the straggling in range has been calculated within the LSS theory for the ion-atom elastic scattering process but not for the inelastic processes, for which it is presumed small.

In the present experiment we have determined from  $\gamma$ -ray-yield measurements using the  $^{14}\text{N}(p,\gamma)^{15}\text{O}$  resonance reaction, the range and distribution profiles of 800-keV singly charged positive  $^{14}\text{N}$  ions implanted in metals from titanium ( $Z_2 = 22$ ) to germanium ( $Z_2 = 32$ ). For these distributions we have determined the values of the first three moments, quantities which are most readily interpretable in terms of theoretical analysis. We have also inferred values for the electronic stopping power and its behavior as a function of the target  $Z_2$ .

The motivation for this investigation arose from experimental results which relate to the converse problem, the dependence of the electronic stopping power on the atomic number of ions incident on a target of fixed  $Z$ . In an accumulation of experiments, the stopping power of ions at constant velocity in the range from lithium ( $Z_1 = 3$ ) to krypton ( $Z_1 = 36$ ) was measured both in amorphous carbon targets<sup>4,5</sup> and in silicon targets in two diffe-

ent channelling directions.<sup>6</sup> The electronic stopping power was found to exhibit a characteristic oscillatory behavior as a function of  $Z_1$ . The positions of the maxima and minima were roughly independent of target material. The question therefore arises as to whether there exists a similar behavior for a single species of incident ion as a function of the target atomic number. Experiments using protons and  $^4\text{He}$  ions show a  $Z_2$  oscillation in the electronic stopping power over a wide range of targets.<sup>7</sup> Some evidence for similar behavior for heavier ions has been presented by Hvelplund<sup>8</sup> for 200-keV  $^{16}\text{O}$  ions for targets from  $Z=2$  to 18 based on a collection of results by several investigators.

The possibility of such oscillatory behavior has some interesting consequences as it relates to the structure of models which describe the electronic stopping. The models developed by Lindhard *et al.*<sup>3</sup> and by Firsov<sup>9</sup> predict a smooth behavior as a function of both  $Z_1$  and  $Z_2$ . However, extensions by several authors<sup>10-14</sup> of the Firsov model, which take into account the atomic structure of both incident ion and target atom, have shown the existence of the  $Z_1$  oscillations and are in qualitative agreement with the experimental results, at least with regard to the positions of the maxima and minima. A calculation of Rouseau, Chu, and Powers<sup>15</sup> for incident  $\alpha$  particles of 800 keV to 2 MeV also shows an oscillating behavior, with the oscillations decreasing as the energy increases. This calculation is based upon the Lindhard theory in which Hartree-Fock-Slater wave functions are used to describe the target atom.

In Sec. II we discuss the experimental method including the use of the profiling technique and target preparation. In Sec. III, the data analysis procedures that we employ are discussed. The results of the experiment, including the distribution profiles which we obtain are presented in Sec. IV. Section V contains a discussion of these results and some conclusions.

## II. EXPERIMENTAL METHODS

The nuclear-resonance reaction of  $^{14}\text{N}(p, \gamma)^{15}\text{O}$  was used to determine the distribution profiles in this study. The measurement of the  $\gamma$ -ray yield as a function of incident proton energies was used to determine the distribution of implanted ions. Details of the method by which the  $\gamma$ -ray-yield data are analyzed are discussed below.

Nuclear-resonance reaction measurements have been successfully used for accurate determination of distribution profiles in a variety of problems. The  $^{19}\text{F}(p, \alpha\gamma)^{16}\text{O}$  reaction has been used to deter-

mine the distribution of fluorine in zircaloy by Möller and Starfelt.<sup>16</sup> The  $^{18}\text{O}(p, \alpha)^{15}\text{N}$  reaction was used by Amsel and Samuel<sup>17</sup> to study anodic oxidation mechanisms and by Whitton and Mitchell<sup>18</sup> to measure the distribution of  $^{18}\text{O}$  implanted in gallium phosphide. Dunning *et al.*<sup>19</sup> have made measurements of aluminum implanted in silicon and silicon compounds using the sharp  $^{27}\text{Al}(p, \gamma)^{28}\text{Si}$  resonance reaction. Phillips and Read<sup>20</sup> and Barker and Phillips<sup>21</sup> have reported results on  $^{15}\text{N}$  implantations in gold, silver, and nickel.

We shall compare their results to ours in Sec. V.

Both the  $^{14}\text{N}$  implantation and the proton probing of the distribution using the  $(p, \gamma)$  resonance were carried out with the Naval Surface Weapons Center 2.5-MV Van de Graaff accelerator. In both phases contaminant buildup on the targets was minimized by using a liquid-nitrogen cold finger directly in front of the target. Mercury pumps were used, but on the basis of backscattering done on the Fe target, we estimate that there was less than a 1% change in range owing to Hg buildup. No measurements on carbon buildup were taken. An electron suppressor set at -1000 V was used to ensure reliable current integration. During the implantation phase of the experiment the target was rotated about an axis parallel to the beam. While this process does not ensure a uniform lateral implantation distribution, it results in radial symmetry and reduces any abrupt discontinuities in the distribution of the implanted ions. The beam aperture for the implantation was approximately 1.2 cm in diameter, while that for the  $(p, \gamma)$  probe was 0.6 cm in diameter.

The  $^{14}\text{N}$  distributions were measured using the 1061.0-keV resonance in the  $^{14}\text{N}(p, \gamma)^{15}\text{O}$  reaction, which has a resonance width of 4.8 keV and a cross section at resonance of 0.37 mb.<sup>22</sup> During the proton probing, the targets were mounted on a water-cooled holder to minimize target overheating and possible diffusion of the implanted ions. The  $\gamma$  rays were detected by a 7.62-by-7.62-cm-diam NaI detector which was placed 3.0 cm from the target at a  $0^\circ$  angle. The NaI detector was surrounded by 4.5 cm of lead to reduce natural backgrounds. The  $\gamma$ -ray signal was amplified and passed through a single-channel analyzer to a scaler gated by the current integrator. Although the  $^{14}\text{N}(p, \gamma)^{15}\text{O}$  resonance reaction used is very prolific in the emission of  $\gamma$  radiation of lower energies, the setting of the single-channel analyzer to accept only the highest-energy  $\gamma$  ray (8.28 MeV)<sup>23</sup> results in the optimum signal-to-background ratio, since the  $\gamma$ -ray backgrounds from the target materials were minimized. Even so, special target preparations had to be used for some targets to reduce the

backgrounds to acceptable values.

Metallic targets of two types were used. For most cases bulk samples were used, provided their surface condition was sufficiently smooth. For those cases with large  $(p, \gamma)$  backgrounds from the host material, thin targets were prepared by evaporating the target onto a Ta backing, which has a low  $(p, \gamma)$  background in the energy range of interest. The thickness of the targets was obtained by weighing and was required to be at least  $3 \mu\text{m}$  thick. This thickness was sufficient to stop all of the  $^{14}\text{N}$  ions but thin enough to reduce the high  $(p, \gamma)$  backgrounds. All of the targets were at least 99.9% pure. The physical forms and thickness of the targets used were as follows:

*Titanium.*  $3 \mu\text{m}$  thick evaporated on 0.0012-cm Ta foil.

*Vanadium.* 0.025-cm-thick foil.

*Manganese.* Heavy bulk chip mechanically polished.

*Chromium.*  $8 \mu\text{m}$  thick evaporated on 0.0012-cm Ta foil.

*Iron.* 0.025-cm-thick foil.

*Cobalt.* 0.050-cm-thick foil.

*Nickel.* 0.025-cm-thick foil.

*Copper.* 0.025-cm-thick foil.

*Zinc.*  $10 \mu\text{m}$  thick evaporated on 0.012-cm Ta foil.

*Germanium.* Polished single crystal. [This target was placed at an angle of a few degrees with respect to the beam to minimize the chance of channeling during both implant and  $(p, \gamma)$  probing. It was the only target which was not rotated during implantation so that the probability that the target would rotate into a channeling position would be eliminated.]

No measurements were attempted on a gallium target because of its low melting point.

The  $\gamma$ -ray-yield measurements were typically accumulated from six individual sweeps through the energy range of interest. This method was used so that apparent changes in the  $^{14}\text{N}$  distributions which might occur through target overheating would be detected. Throughout all of the measurements, no discernible difference was detected in the  $\gamma$ -ray-yield curves and hence in the concentration distributions for any of the targets. This also tends to rule out extensive contaminant buildup on the target.

The Van de Graaff accelerator was calibrated by using the sharp  $(p, \gamma)$  resonance in aluminum at 991.88 keV. The calibration target was thin  $\text{Al}_2\text{O}_3$  evaporated on a Ni backing. Machine calibrations were conducted before running a  $^{14}\text{N}$  implant and immediately after a  $(p, \gamma)$  probe. These periodic calibration checks showed that the

variance in the incident-beam energy due to the system apertures and the short-term magnet stability was of the order of 300 eV for 1-MeV protons. However, these calibrations also show that there is a long-term variation in the machine calibration of approximately 1 keV over the period of time required to probe the target several times. This variation is reflected in the errors, as discussed below. The  $\gamma$ -ray spectrometer was also calibrated at regular intervals to check for any excessive change in gain and single-channel-analyzer window width.

### III. DATA PROCESSING

Backgrounds from two sources were subtracted from the total  $\gamma$ -ray yield to obtain the contribution from the  $^{14}\text{N}(p, \gamma)^{15}\text{O}$  resonance reaction. There is a time-dependent background originating from natural sources in the detector environment. This background is independent of the proton beam. There is also a charge-dependent background which results from  $(p, \gamma)$  reactions in the host material and from the off-resonance reaction from the  $^{14}\text{N}$ . If, after subtracting the time-dependent background, the charge-dependent background measurements on an unimplanted sample showed a linear increase in the  $\gamma$ -ray yield as a function of proton energy, the charge-dependent background to be subtracted from the  $(p, \gamma)$  signal was taken as a linear curve between high- and low-energy end points of the  $\gamma$ -ray profile measurements. If the background showed a nonlinear behavior, a point-by-point background taken on an unimplanted sample was subtracted from the  $(p, \gamma)$  probe measurements. In this case the background from the unimplanted sample was normalized to that of the implanted sample at the high- and low-energy end points.

After background subtraction, the  $^{14}\text{N}$  concentration distribution must be related to the  $\gamma$ -ray-yield distribution. In order to do this, several processes which broaden the  $\gamma$ -ray yield must be properly taken into account. These processes include:

(a) the finite width of the incident-proton beam, represented by the Gaussian form

$$I(E, E_B) = \frac{N_B}{(2\pi\sigma_B^2)^{1/2}} \exp\left[-\frac{(E - E_B)^2}{(2)\sigma_B^2}\right], \quad (1)$$

where  $I(E, E_B)$  is the intensity at energy  $E$  of a beam of energy  $E_B$ ,  $\sigma_B$  is the variance or spread of the beam, taken to be 300 eV, and  $N_B$  is the fluence of incident protons;

(b) the finite width of the reaction cross section  $\sigma(E)$  at proton energy  $E$ , represented by the Breit-

Wigner resonance cross section

$$\sigma(E) = \frac{\pi\lambda^2}{(2J_p + 1)(2J_i + 1)} \frac{(2J_c + 1)\Gamma_p\Gamma_\gamma}{(E - E_R)^2 + \frac{1}{4}\Gamma^2}, \quad (2)$$

where  $E_R$  is the resonance energy for the  $(p, \gamma)$  reaction.  $J_c$ ,  $J_p$ , and  $J_i$  are the spins of the compound nucleus, the incident proton, and the target state, respectively; and  $\Gamma_p$ ,  $\Gamma_\gamma$ , and  $\Gamma$  are the widths of the incident-proton channel, the exit  $\gamma$ -ray channel, and the compound nucleus, respectively (these values are obtained from the Nuclear Data Tables);

(c) the energy straggling of the proton beam which, at sufficiently deep layers in the target, has the Gaussian distribution function

$$Y(E_B) = Y_0 \int_0^R dR' n(R') \frac{1}{\pi} \int_0^\infty \frac{dE}{E} \frac{\frac{1}{2}\Gamma}{(E - E_B)^2 + \frac{1}{4}\Gamma^2} \int_0^\infty dE' \frac{1}{[2\pi\sigma_B^2 2\pi\sigma_B^2(R')]^{1/2}} \exp\left[-\left(\frac{(E - E_B)^2}{2\sigma_B^2} + \frac{[E - \mathcal{G}(E', R)]^2}{2\sigma_B^2(R')}\right)\right],$$

where  $Y_0 = \frac{1}{4}\Gamma\sigma_R E_R \omega N_t f_c f_\gamma$ ,  $\sigma_R$  is the cross section at resonance,  $N_t$  the target thickness in particles/cm<sup>2</sup>,  $f_c$  the detection efficiency for the  $\gamma$  ray, and  $f_\gamma$  the  $\gamma$ -ray branching ratio.

The function  $n(r)$  is the concentration distribution function which gives rise to the measured  $\gamma$ -ray-yield curves. This function is frequently taken to be a Gaussian probability distribution

$$n(R) = \frac{1}{\sqrt{(2\pi)\Delta R_p}} \exp\left[-\left(\frac{R - R_p}{\sqrt{(2)\Delta R_p}}\right)^2\right], \quad (4)$$

where  $R_p$  and  $\Delta R_p$  are the projected range and range straggling for the implanted ions obtained from the LSS theory. However, to account for a possible asymmetry in the observed distributions, we have taken  $n(R)$  to be combined left and right half-Gaussian curves of different widths  $\Delta R_-$  and  $\Delta R_+$ , matched in amplitude at the peak position  $R_{\text{peak}}$ .<sup>24</sup> The parameters for the split-Gaussian distribution are obtained from a least-squares fit to the measured  $\gamma$ -ray-yield data  $Y(E_B)$ .

In this analysis, the stopping power and energy straggling of the protons in the target material is required. The values of the proton stopping powers for the elements of interest were obtained from Bichsel.<sup>25</sup> The proton stopping used was that for the pure metallic elements. The effect of the implanted nitrogen is discussed below. The proton straggling was taken from calculations by Chu and Mayer,<sup>26</sup> based on the Bonderup and Hvelplund<sup>27</sup> modification of the Lindhard-Scharff theory.<sup>28</sup> These values are related to the Bohr expression for the straggling by

$$\sigma_E^2 = C\sigma_{E, \text{Bohr}}^2(R),$$

$$F(E, E', R) = \frac{1}{[2\pi\sigma_E^2(R)]^{1/2}} \exp\left[-\left(\frac{E - \mathcal{G}(E', R)}{\sqrt{(2)\sigma_E(R)}}\right)^2\right], \quad (3)$$

where  $\mathcal{G}(E', R)$  is the average energy of a proton of initial energy  $E'$  at target depth  $R$  and is obtained from

$$R = \int_{E'}^{\mathcal{G}(E', R)} \frac{dE''}{dE/dR},$$

and  $\sigma_E(R)$  is the variance in energy owing to the straggling of the proton beam at depth  $R$ . Combining Eqs. (1)–(3) we find, for the counting rate of  $\gamma$ -rays emitted into a solid angle  $\omega$  per incident proton,

where the correction factor  $C$  is of the order of 0.75 at 1 MeV for the elements of interest, and

$$\sigma_{E, \text{Bohr}}^2(R) = 4\pi e^4 N Z_2 R.$$

#### IV. RESULTS

Metallic targets of titanium ( $Z_2 = 22$ ) through germanium ( $Z_2 = 32$ ), with the exception of gallium, were implanted with 800-keV  $^{14}\text{N}$  ions at fluences of the order of  $10^{17}$  ions/cm<sup>2</sup>. The resulting distributions were profiled utilizing the 1061.0-keV resonance of width 4.8 keV from the  $^{14}\text{N}(p, \gamma)^{15}\text{O}$  reaction. The results of these measurements are given in Fig. 1, where the relative  $\gamma$ -ray yield is shown as a function of the incident proton energy relative to the 1061.0-keV resonance. All of the

TABLE I. Peak positions and widths (full width at half-maximum) in keV of  $\gamma$ -ray-yield curves from the  $^{14}\text{N}(p, \gamma)^{15}\text{O}$  resonance reaction of  $^{14}\text{N}$  implanted in targets from titanium through germanium.

Element	$Z_2$	Peak		Width (FWHM)	
		Expt.	LSS	Expt.	LSS
Titanium	22	48	65	28.0 ± 4.0	29
Vanadium	23	48	64	18.5 ± 2.5	31
Chromium	24	47	64	20.5 ± 2.5	31
Manganese	25	56	64	16.0 ± 5.0	31
Iron	26	56	64	23.0 ± 3.0	32
Cobalt	27	60	64	25.5 ± 3.5	33
Nickel	28	62	64	28.0 ± 1.5	33
Copper	29	66	64	27.5 ± 4.5	34
Zinc	30	68	64	32.5 ± 4.0	34
Germanium	32	58	64	27.0 ± 2.0	36

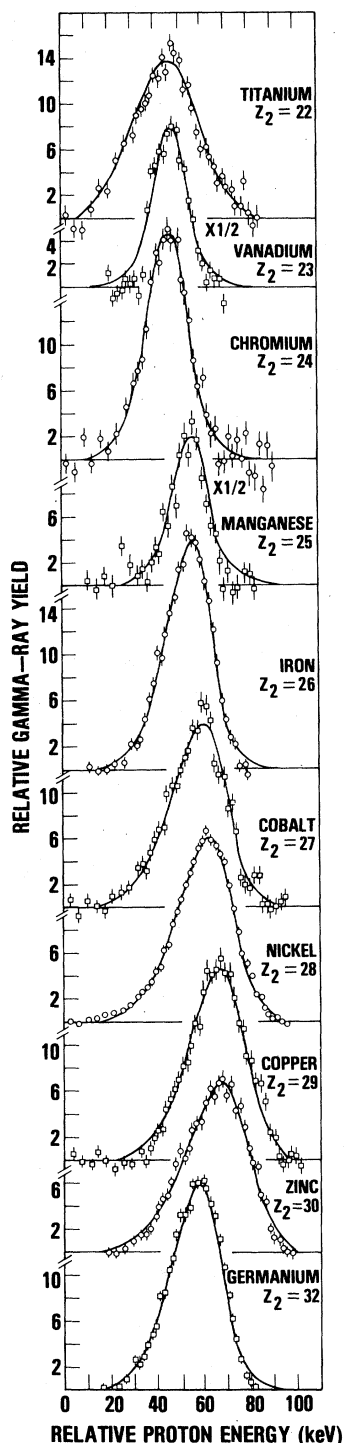


FIG. 1.  $\gamma$ -ray-yield distributions for 800-keV  $N^+$  ions implanted in metallic targets for  $Z=22-32$  obtained from the  $^{14}N(p,\gamma)^{15}O$  resonance reaction at 1061.0 keV. Error bars are counting errors only. Solid curves, least-squares-fit  $\gamma$ -ray-yield curves obtained from split-Gaussian distributions. All curves are normalized to the same area.

distributions are normalized to the same area. The errors in the measured yield distributions are counting errors only. The solid curves shown in Fig. 1 are calculated yield curves obtained from the least-squares fit to the data assuming the split-Gaussian concentration for the implanted ions described above. Clearly, the fits are excellent. The energy positions of the peak and the full width at half-maximum (FWHM) of the measured yield distributions are given in Table I and Fig. 2, which also give these quantities obtained from concentration distributions calculated from the LSS theory.<sup>29</sup> The errors in the experimental peak positions reflect the long-term variation of the machine energy of about 1 keV as well as counting errors. These peak positions are lower from those expected from theory by as much as 30%, and the measured widths are narrower by as much as 40%. The greatest deviations occur for the targets with lower atomic numbers.

The concentration distributions obtained from the least-squares fit to the  $\gamma$ -ray-yield distributions (Fig. 1) are shown in Fig. 3. The dashed curves are those predicted by the LSS theory in which the Gaussian distribution of Eq. (4) is assumed. All of the curves are normalized to the same peak height for ease in comparison of the distribution shapes. A summary of the positions of the peak of the concentration distributions and widths of the split Gaussian in  $mg/cm^2$  is given in Table II. The distributions are generally shallower and narrower than those predicted by theory. In addition, we note that the concentration distributions are not symmetric but skewed such that, from the peak position, all distributions decrease more

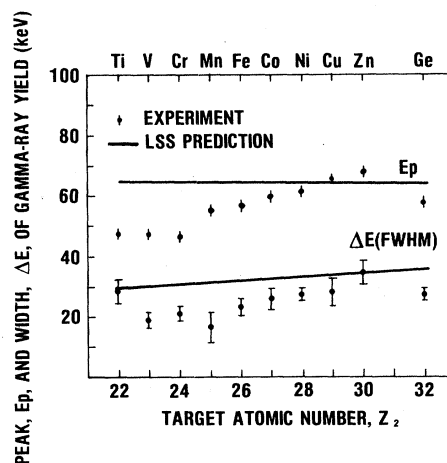


FIG. 2. Peak positions,  $E_p$ , and widths,  $\Delta E_p$ , of the  $\gamma$ -ray-yield distribution as a function of the target atomic number,  $Z_2$ . The errors in  $E_p$  reflect errors in machine energy as well as counting errors. The solid curves are those predicted by the LSS theory.

rapidly toward the deeper depths than toward the surface. No explanation is immediately available as to why the width is so large for titanium,  $Z_2 = 22$ , but the effect is apparently real and not an experimental error.

The values of the peak position  $R_{\text{peak}}$  and split-Gaussian widths,  $\Delta R_-$  and  $\Delta R_+$ , of the  $^{14}\text{N}$  concentration function (Table II) should not be compared directly with the values of the projected range and range straggling obtained from the LSS theory, since the latter are the first and second

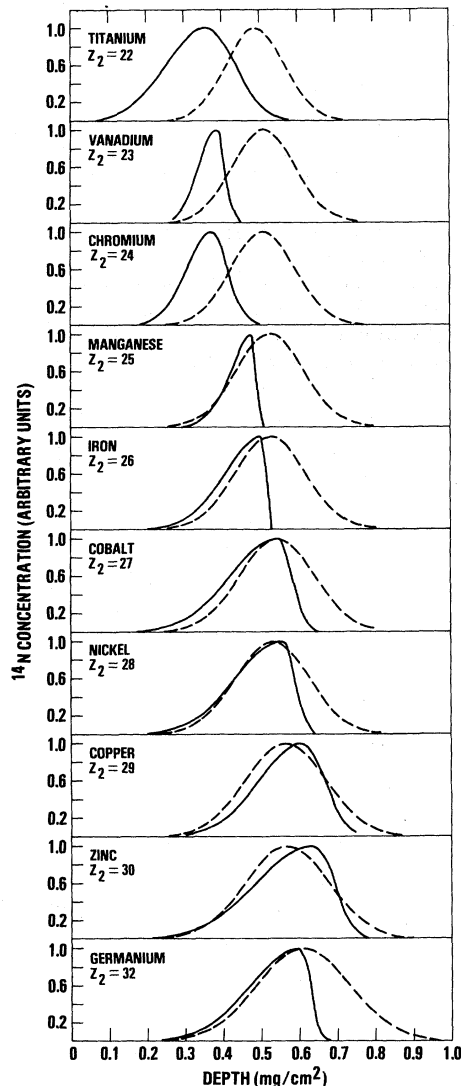


FIG. 3. Concentration distributions of 800-keV  $^{14}\text{N}^+$  ions implanted in metallic targets for  $Z = 22$ – $32$ . The solid curves are split-Gaussian functions which result in the least-squares fit to the  $\gamma$ -yield curves. The dashed curves are the distributions predicted by the LSS theory. All curves are normalized to the same peak height.

moments of the distribution. The moments derived from the experimental measurements as well as the corresponding LSS predictions are also given in Table II and shown in Fig. 4 as a function of the atomic number  $Z_2$ . In addition, the experimental values of the third moments of the concentration distributions which relate to their skewness are also given in Table II. The negative values indicate that the distributions have greater weight on the left-hand (or negative) side of the peak.

The representations of the concentration profile by a split Gaussian sets a limitation of the magnitude of the third moment which can be accommodated. This limit arises from the obvious requirement that the widths  $\Delta R_{\pm}$  be positive. We have chosen a lower limit for  $\Delta R_{\pm}$  of  $0.005 \mu\text{m}$ . The first three moments of the distribution are, in fact, not particularly sensitive to a single small value of either  $\Delta R_+$  or  $\Delta R_-$ . Although the lower limit of  $\Delta R_+ = 0.005 \mu\text{m}$  was required for several implantations, the details of our calculations suggest that the third moment of the experimental distribution is not significantly larger than the maximum value the split-Gaussian representation can describe.

The peak of the concentration distributions ob-

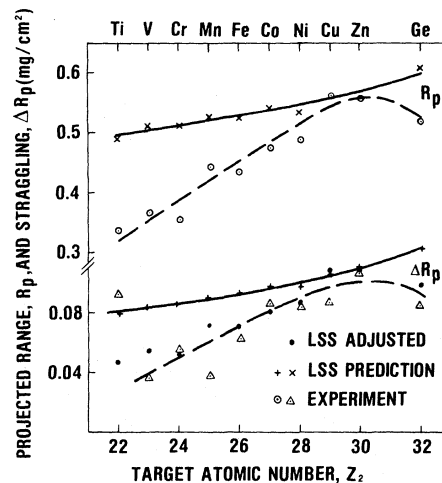


FIG. 4. Projected range,  $R_p$ , and straggling,  $\Delta R_p$ , for 800-keV  $^{14}\text{N}^+$  ions implanted in targets of atomic numbers ranging from  $Z_2 = 22$  through  $Z_2 = 32$ . The curves are drawn here to guide the eye, with the solid curves representing the LSS prediction and the dashed curves the experimental results. The experimental points are the first and second moments of the experimental  $^{14}\text{N}$  concentration distributions. The LSS adjusted points are resulting straggling values when the adjusted electronic stopping power is used in the LSS theory. In this case the first moments are equal to the experimental first moments.

tained here are determined to an accuracy of about 200 Å. That is, if the peak position of the concentration distribution were changed by about 200 Å, an easily discernible difference would be observed in the calculated yield distributions when compared with the measured distributions. This accuracy is not to be construed as the resolution of the  $(p, \gamma)$  resonance reaction technique for determining  $^{14}\text{N}$  concentration distributions. This resolution is interpreted as the system resolution and is due to all processes which broaden the measurement for the determination of the position of a thin layer of  $^{14}\text{N}$  atoms in the host material by the  $(p, \gamma)$  resonance reaction. The major processes which contribute to this broadening are the energy straggling of the proton beam as it passes through the target, the energy width of the  $(p, \gamma)$  resonance reaction, and the energy width of the incident-proton beam before it enters the target. Of these, only the energy straggling is a function of the depth of the  $^{14}\text{N}$  in the host material, and eventually it becomes the dominant contribution to a decrease in resolution for deep implants. At the depths determined for the  $^{14}\text{N}$  implantation here, this is the major contribution to the resolution. The FWHM resolution of the system for  $^{14}\text{N}$  at a depth of 0.65  $\mu\text{m}$  in Fe is about 1450 Å.

The influence of the changing resolution as a function of depth for determining the concentration distribution of  $^{14}\text{N}$  in Fe is demonstrated in Fig. 5, where the concentration distribution and the yield distribution are both shown. Both curves are normalized to the same area. The difference in these two distribution curves is attributed to the above mentioned factors which broaden the yield distribution. We note from Fig. 5 that the two curves agree more closely at the low-energy

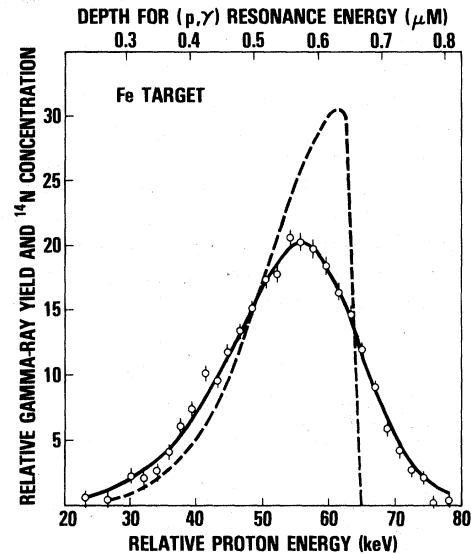


FIG. 5. Comparison between the  $\gamma$ -ray-yield distributions (solid curve) and the concentration distributions (dashed curve) for 800-keV  $^{14}\text{N}^+$  ions implanted in Fe. Areas under both curves are normalized to the same value. The differences in the curves are primarily due to proton straggling effects, although some contribution is due to the width of the  $(p, \gamma)$  resonance curve and the width of the incident-proton beam. If all widths were  $\delta$  functions, the shapes of the curves would be identical.

(shallow) side of the distribution than at the high-energy (deep) side. This difference is a direct consequence of the increasing energy straggling of the proton beam as it penetrates deeper into the target. If all the processes which spread the  $\gamma$ -ray-yield distributions were  $\delta$  functions (i.e., very sharply peaked), the shapes of the concentrations curves and yield curves would be identical.

TABLE II. Experimental and theoretical distribution parameters of 800-keV  $^{14}\text{N}$  implanted in metallic targets from titanium through germanium (all values are in  $\text{mg}/\text{cm}^2$ ).

Element	$Z_2$	Concentration distribution			First moment <sup>a</sup>		Second moment <sup>b</sup>			Third moment $(\Delta R_{3p})^{1/3}$
		$R_{\text{peak}}$	$\Delta R_-^c$	$\Delta R_+^d$	$R_p^{\text{expt}}$	$R_p^{\text{LSS}}$	$\Delta R_p^{\text{expt}}$	$\Delta R_p^{\text{LSS}}$	$\Delta R_p^{\text{ADJ}}$	
Titanium	22	0.361	0.107	0.076	0.336	0.490	0.092	0.078	0.046	-0.059
Vanadium	23	0.388	0.048	0.022	0.367	0.511	0.036	0.083	0.054	-0.029
Chromium	24	0.373	0.066	0.044	0.355	0.509	0.055	0.084	0.051	-0.038
Manganese	25	0.487	0.062	0.004	0.441	0.527	0.037	0.090	0.071	-0.038
Iron	26	0.509	0.100	0.004	0.433	0.525	0.061	0.092	0.071	-0.061
Cobalt	27	0.546	0.124	0.035	0.474	0.543	0.085	0.097	0.080	-0.077
Nickel	28	0.560	0.123	0.031	0.487	0.530	0.082	0.097	0.086	-0.076
Copper	29	0.608	0.113	0.057	0.563	0.564	0.087	0.106	0.107	-0.068
Zinc	30	0.639	0.150	0.050	0.559	0.568	0.106	0.110	0.108	-0.093
Germanium	32	0.601	0.128	0.025	0.518	0.611	0.084	0.123	0.098	-0.080

<sup>a</sup> Projected range.

<sup>b</sup> Straggling.

<sup>c</sup> Width of left-hand side of split-Gaussian distribution.

<sup>d</sup> Width of right-hand side of split-Gaussian distribution.

cal, and the ( $p, \gamma$ ) resonance measurement would provide a direct mapping of the concentration distribution.

The deviations between the measured concentrations and the predicted LSS distributions as shown in Fig. 4 suggest that stopping powers greater than those used in the theory are needed to predict the distribution more accurately. Since the electronic stopping power  $S_e$  is dominant over the nuclear stopping power  $S_n$  from the implant energy of 800 keV down to about 30 keV, it appears that an alteration of this quantity is required to bring the theoretical values into agreement with the measured values. The change in  $S_e$  can be further justified in the present instance by examining the effects of a change in  $S_n$ . Consider Fig. 6, which shows the dependence of both the projected range and range straggling on the energy of the incident ions as predicted by the LSS theory. These curves are determined for a case in which the electronic stopping power is fixed and the nuclear power is taken to be 0.1, 1.0, and 2.0 times the LSS value for  $^{14}\text{N}$  ions implanted in iron. Recalling that both the projected range and the width of the measured distributions are smaller than those predicted by the LSS theory, we see that both cannot be decreased as required by the experimental values by a change in  $S_n$ . In order to decrease significantly the projected range for 800-keV  $^{14}\text{N}$  ions, a large increase in  $S_n$  is needed. However, from Fig. 6 we see that at this energy the effect of a large increase in  $S_n$  is to in-

crease the straggling slightly rather than to decrease it significantly as needed. An increase in  $S_e$  does decrease both the projected range and range straggling; therefore, we conclude that it is the behavior of  $S_e$  that must be modified.

It should be noted from Fig. 6 that this conclusion would not necessarily be the case at implant energies below about 100 keV. At this energy an increase in  $S_n$  would decrease both the projected range and the straggling. These decreases are brought about by the fact that, even though  $S_n$  is the dominant influence on the straggling through wide-angle scattering processes and an increase might be thought to increase the straggling, the implanted ions are stopped more quickly such that they do not experience as many wide-angle scattering collisions before they are brought to rest. Thus, the projected range and straggling are both decreased.

The values of the electronic stopping power, adjusted such that the theoretically determined values of the projected ranges are equal to the experimental values, are displayed in Fig. 7 and listed in Table III as a function of  $Z_2$ . The changes in  $S_e$  are made by altering the LSS value of  $S_e$  by a multiplicative constant. Therefore, this change does not alter the linear dependence of  $S_e$  on the velocity of the incident particle. Figure 7 shows that increases in  $S_e$  by as much as 60% are needed to account for the measured distributions, and that  $S_e$  exhibits a  $Z_2$  dependence which is not accounted for in the Lindhard<sup>3</sup> or Firsov<sup>9</sup> pictures

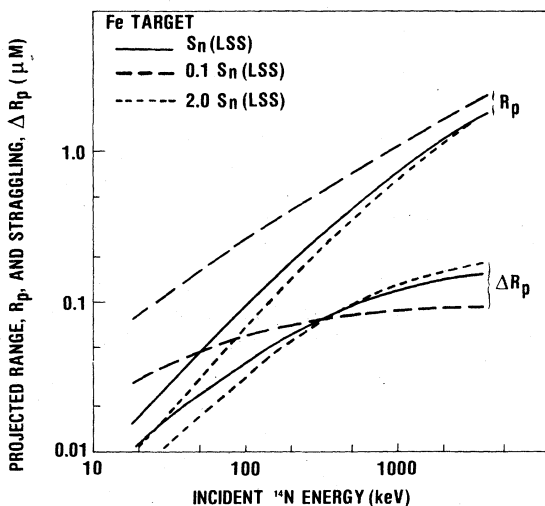


FIG. 6. Variation of the projected range,  $R_p$ , and the straggling,  $\Delta R_p$ , for  $^{14}\text{N}^+$  ions incident on an Fe target for cases in which the nuclear stopping power  $S_n$  is equal to 0.1, 1.0, and 2.0 times the LSS value of  $S_n$ . At energies above about 100 keV, an increase in  $S_n$  is reflected by a decrease in  $R_p$  but by an increase of  $\Delta R_p$ .

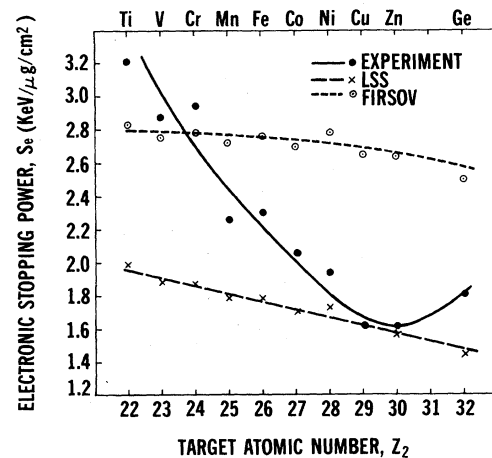


FIG. 7. Experimental, LSS, and Firsov values for the electronic stopping power for 800-keV  $^{14}\text{N}^+$  ions as a function of the target atomic number  $Z_2$ . The curves are drawn to guide the eye. The experimental values are obtained by altering the LSS value by a multiplicative constant such that the first moment from the LSS transport theory is in agreement with the experimental values of the concentration distribution.

TABLE III. Values of the electronic stopping powers in keV/( $\mu\text{g}/\text{cm}^2$ ) for 800-keV  $^{14}\text{N}$  in metallic targets from titanium through germanium as inferred from the projected range of this experiment and from theories of LSS and of Firsov.

$Z_2$	$S_e$ (Expt.)	$S_e$ (LSS)	$S_e$ (Firsov)
22	3.22	1.99	2.84
23	2.88	1.89	2.76
24	2.95	1.88	2.79
25	2.27	1.80	2.73
26	2.31	1.79	2.77
27	2.06	1.72	2.70
28	1.95	1.74	2.79
29	1.63	1.63	2.66
30	1.63	1.60	2.65
32	1.81	1.46	2.51

of electronic stopping.

The calculation of the profile parameter  $R_p$  from the adjusted values of  $S_e$  also results in adjusted values of the straggling (LSS adjusted). The values of  $\Delta R_p$  (LSS adjusted) are also shown in Fig. 4 and in Table II. It should be noted that these values follow the measured values much more closely than those obtained from the LSS theory.

## V. DISCUSSION

In this investigation we have shown that the concentration profiles in Fig. 3 differ from those expected on the basis of theory in that they are shallower and narrower. In addition, they are generally rather strongly skewed, decreasing from the peak more rapidly toward deeper layers of the target. We have presented our results for the profiles in terms of their moments, since these quantities are directly associated with the theory.

From these results we have concluded that the electronic stopping power displays a systematic deviation from that value predicted by either the Lindhard or Firsov models. Because of the limited range of targets investigated here, we cannot firmly conclude the existence of oscillations in  $S_e$  as a function of  $Z_2$ . However, there is good evidence for this behavior. It shows a minimum in the vicinity of Cu ( $Z=29$ ) which is in agreement with the previously observed oscillation in the  $Z_1$  dependence of  $S_e$  and the  $Z_2$  dependence for incident light ions.

Since these targets are implanted with relatively high fluences such that the highest atomic density is about 10% of the host material, some concern should be given to the possibility of a fluence effect on the measured concentration distributions. The implantation of heavy particles in a host ma-

terial causes a change in the stopping power as well as straggling of that material from the addition of the particles themselves and possibly from the damage inflicted on the material by the implantation. This change is effective both during implantation and during proton profiling. We have made a measurement of the  $^{14}\text{N}$  concentration distribution in which implantation in Fe was carried out at a fluence of one-tenth that normally used in this experiment. The concentration profiles for the two cases of fluence differing by a factor of 10 are not appreciably different. Thus, we conclude that the effects of fluence are not significant to the results of this experiment.

Estimates of the effect of the added stopping power in the implanted region during proton profiling can easily be made. This added stopping causes the protons to lose additional energy, and hence the values obtained for both first and second moments are larger than what they would be in the absence of the added stopping. That is, the profiles appear to be deeper and wider than they really are. We have estimated that the effect of the additional stopping of the protons by the implanted  $^{14}\text{N}$  results in an overestimation of the projected range by no more than 1%. This difference results in a minor correction in the determination of the electronic stopping power of the  $^{14}\text{N}$ . Furthermore, the apparent width of the concentration distribution is estimated to be of the order of 5% wider than what would be obtained if the additional proton stopping were included in the analysis. No definite conclusions can be reached easily for the skewness.

Thus we see that our analysis provides, in a rigorous sense, an upper bound on the profile width. Other approximations also support this result. Harris and Nicolet<sup>30</sup> suggest that the values of Chu and Mayer may underestimate the true proton straggling. The long-term variation of the Van de Graaff accelerator energy would also broaden the observed peak. Nevertheless, the widths of the concentration profiles obtained from this investigation are significantly narrower than the theoretical predictions, and the effects discussed here would only widen the gap.

In the description of the theory of range and range straggling presented in Sec. I, we distinguished between the transport theory and the theory of the atomic cross sections. In our analysis we attributed the deviations between the experimental and the theoretical results to the electronic stopping power alone, and we have assumed that the nuclear stopping power as well as the expressions for the projected range and range straggling are both accurately represented within the context of this study. We have previously shown that

the range and straggling are relatively insensitive to one type of variation of the nuclear stopping. We may also argue that our analysis should not be sensitive to the transport theory. Since we are concerned with a series of elements in the same region of the periodic table, the values we have found for the first and second moments should be at least consistent relative to one another.

Some specific evidence for the validity of our analysis of the electronic stopping power may be found in a comparison between our measurements of this quantity for  $^{14}\text{N}$  and Ni and some corresponding measurements of Porat and Ramavataram.<sup>31</sup> These authors have measured the electronic stopping power through the energy loss of both  $^{14}\text{N}$  and  $^{20}\text{Ne}$  beams through thin metallic foils at several energies. Their results for 800- and 1200-keV  $^{14}\text{N}$  ions on Ni are 2.06 and 2.52 keV/ $(\mu\text{g}/\text{cm}^2)$ , respectively. These values are to be compared with our values of 1.95 keV/ $(\mu\text{g}/\text{cm}^2)$  at 800 keV and 2.43 keV/ $(\mu\text{g}/\text{cm}^2)$  at 1200 keV. The close agreement between these quantities obtained by two entirely different experimental methods gives further confidence to our working hy-

potheses that the effects of the nuclear stopping are being adequately accounted for and that the fluence effects discussed above are small.

It is interesting to compare our results for  $^{14}\text{N}$  on Ni with the results of Barker and Phillips<sup>21</sup> for  $^{15}\text{N}$  on Ni. There is reasonably good agreement in stopping power but relatively poor agreement in the width of the distributions. This is, perhaps, not too surprising, since Barker and Phillips do not unfold the concentration profile from their yield curves by including the effect of proton straggling. This tends to make their stopping power smaller than ours and their straggling larger.

#### ACKNOWLEDGMENTS

The authors would like to thank John Mays for his assistance in making the measurements and T. Orlow for some advice on the data processing. In addition, they wish to thank Dr. G. Hubler and Dr. K. Dunning for their helpful discussions on the resonance-reaction technique and Dr. Hans Bichsel for his guidance in obtaining proton stopping powers.

\*Also at Catholic University of America, Washington, D. C. 20017.

<sup>1</sup>J. Lindhard, M. Scharff, and H. E. Schiott, K. Dan. Vidensk. Selsk. Mat.-Fys. Medd. **33**, No. 14 (1963).

<sup>2</sup>J. Lindhard, V. Nielson, and M. Scharff, K. Dan. Vidensk. Selsk. Mat.-Fys. Medd. **36**, No. 10 (1968).

<sup>3</sup>J. Lindhard and M. Scharff, Phys. Rev. **124**, 128 (1961).

<sup>4</sup>J. H. Ormrod, J. R. MacDonald, and H. E. Duckworth, Can. J. Phys. **43**, 275 (1965).

<sup>5</sup>P. Hvelplund and B. Fastrup, Phys. Rev. **165**, 408 (1968).

<sup>6</sup>F. H. Eisen, Can. J. Phys. **46**, 561 (1968).

<sup>7</sup>M. Bader, R. E. Pixley, F. S. Mozer, and W. Whaling, Phys. Rev. **103**, 32 (1965); D. Wayne Green, John N. Cooper, and James C. Harris, *ibid.* **98**, 466 (1955); W. K. Lin, H. G. Olson, and D. Powers, Phys. Rev. B **8**, 1881 (1973); and W. K. Chu and D. Powers, Phys. Rev. **187**, 478 (1969).

<sup>8</sup>P. Hvelplund, K. Dan. Vidensk. Selsk. Mat.-Fys. Medd. **38**, No. 4 (1971).

<sup>9</sup>O. B. Firsov, Zh. Eksp. Teor. Fiz. **36**, 1517 (1959) [Sov. Phys.—JETP **36**, 1076 (1959)].

<sup>10</sup>I. M. Cheshire, G. Dearnaley, and J. M. Poate, Proc. R. Soc. A **311**, 47 (1969).

<sup>11</sup>C. P. Bhalla and J. N. Bradford, Phys. Lett. **27A**, 318 (1968).

<sup>12</sup>C. P. Bhalla, J. N. Bradford, and G. Reese, in *Atomic Collision Phenomena in Solids*, edited by D. W. Palmer, M. W. Thompson, and P. D. Townsend (North-Holland, Amsterdam, 1970), p. 361.

<sup>13</sup>K. B. Winterbon, Can. J. Phys. **46**, 2429 (1968).

<sup>14</sup>A. H. El-hoshy and J. F. Gibbons, Phys. Rev. **173**, 454 (1968).

<sup>15</sup>C. C. Rousseau, W. K. Chu, and D. Powers, Phys. Rev. A **4**, 1006 (1971).

<sup>16</sup>E. Möller and N. Starfelt, Nucl. Instrum. Methods **50**, 225 (1967).

<sup>17</sup>G. Amsel and D. Samuel, J. Phys. Chem. Solids **23**, 1707 (1962).

<sup>18</sup>J. L. Whitton and I. V. Mitchell, Can. J. Phys. **49**, 1225 (1971).

<sup>19</sup>K. L. Dunning, G. K. Hubler, J. Comas, W. H. Lucke, and H. L. Hughes, Thin Solid Films **19**, 145 (1973).

<sup>20</sup>W. R. Phillips and F. H. Read, Proc. Phys. Soc. Lond. **81**, 1 (1963).

<sup>21</sup>P. H. Barker and W. R. Phillips, Proc. Phys. Soc. Lond. **86**, 379 (1965).

<sup>22</sup>P. M. Endt and C. Van der Leun, Nucl. Phys. **A214**, 205 (1973).

<sup>23</sup>A. E. Evans, B. Brown, and J. B. Marion, Phys. Rev. **149**, 863 (1966).

<sup>24</sup>J. F. Gibbons and S. Mylroie, Appl. Phys. Lett. **22**, 563 (1973).

<sup>25</sup>H. Bichsel, *American Institute of Physics Handbook*, 3rd ed. (McGraw-Hill, New York, 1972), Sec. 8D, pp. 8-142.

<sup>26</sup>W. K. Chu and J. W. Mayer (unpublished).

<sup>27</sup>E. Bonderup and P. Hvelplund, Phys. Rev. A **4**, 562 (1971).

<sup>28</sup>J. Lindhard and M. Scharff, K. Dan. Vidensk. Selsk. Mat.-Fys. Medd. **27**, No. 15 (1953).

<sup>29</sup>Calculations of the projected range and range straggling described in this paper were performed with a computer code written by H. E. Schiott [Can. J. Phys. **46**, 449 (1968)] and most graciously provided to us by him.

<sup>30</sup>J. M. Harris and M. A. Nicolet, Phys. Rev. B **11**, 1013 (1975).

<sup>31</sup>D. I. Porat and K. Ramavataram, Proc. Phys. Soc. Lond. **78**, 1135 (1961).